Journal of Petroleum Science and Technology 10 (2020) 2-11
DOI:10.22078/jpst.2020.4060.1647

Journal of Petroleum Science and Technology

https://jpst.ripi.ir/

Reaction Kinetics of MoCo/Al_2O_3-Meso-ZSM-5 Catalyst for Ultra-Deep Hydrodesulfurization of Diesel Fuel

Liu Li*, Yang Chengmin, Duan Weiyu, Sun Jin, Yao Yunhai, Li Shicai, and Guo Rong
Dalian Research Institute of Petroleum and Petrochemicals, SINOPEC, Dalian, China

Abstract

Series of Mo-Co type catalysts were supported on Al_2O_3, Al_2O_3-meso-ZSM-5-Al_2O_3-typical-ZSM-5 and tested in the hydrodesulfurization (HDS) of straight-run diesel feedstocks. The materials were characterized by N_2 physisorption, X-ray diffraction, scanning electron microscopy, NH_3 adsorption and temperature-programmed desorption, and Py-adsorbed IR spectra. The dynamics of the main steps in the HDS reaction were calculated, and seven lumped kinetic equations were established containing reaction pathways of hydrogenation (HYD), direct desulfurization (DDS) and alkyl transfer on the catalyst. The Levenberg-Marquardt (LM) algorithm method was used then to solve the resulting differential equations. The results showed that the HDS activity of C12-ZSM5 was highest because it had large V_P and D_P, and moderate acid content, which could improve the alkyl transfer activity and the macromolecular sulfide diffusion. By increasing the operating temperatures, the sulfur removal through the alkyl transfer route on C12-ZSM5 catalyst significantly increased, and the removal of sulfur content through alkyl transfer at 400 °C and 4.0 MPa or 6.0 MPa was 86 or 88%, respectively. Furthermore, the increase of sulfur removal confirmed that the alkyl transfer route was dominant at a deep HDS level at a high operating temperature.

Key words: Mo-Co Type Catalyst, ZSM Zeolite, Hydrodesulfurization, Kinetics.

Introduction

Recent legislation in many countries concerning air pollution by diesel exhaust gas prompts refiners to reduce the sulfur content of gas oil. Many countries are beginning to implement ultra-low sulfur diesel (ULSD <10 ppm sulfur), alkyldibenzothiophenes with side chains in sterically hindering positions need to be removed [1]. However, these molecules and especially compounds substituted in the 4 and/or 6 positions are refractory to the hydrodesulfurization (HDS) process, because of the two substituents on the beta site [2,3]. For the sulfur compounds, the high conversions can be achieved by using expensive and drastic methods such as increasing the temperatures and the pressure in the reactor, lowering the liquid hourly space velocity, or increasing the new reactors [4]. The development of a new catalyst is an economical and effective method for refiners and catalyst producers, and it could be more easily achieved by a better knowledge of the ultra-deep HDS process [5]. In order to develop a catalyst having a super high HDS activity, the kinetic reaction of the alkyldibenzothiophene derives such as 4, 6-Dimethyl-dibenzothiophene (4, 6-DMDBT) removal should be thoroughly studied.

Much researches have been performed to find out the transformation mechanism of 4, 6-DMDBT species [6-8]. The 4, 6-DMDBT species are more inclined to be transformed according to the hydrogenation (HYD) pathway rather than the direct desulfurization (DDS) pathway, in relation to methyl steric hindrance [9,10], and kinetics investigations of the behavior have led to contradictory explanations. The first hypothesis suggests that the transformation of 4, 6-DMDBT is limited by the adsorption step. In this case, the alkyl groups sterically hinder adsorption [11]. Moreover, the second proposal assumes that the elimination step is hindered by steric effects [12,13]. Furthermore, according to the study carried out by Vrinat et al., it was found out that the drastic decrease in the reaction rate of 4, 6-DMDBT does not relate to adsorption. Still, a steric hindrance in the elimination reaction involves the C–S bond scission [8]. Also, according to the study which has been carried out by Guo et al., it has been found out that the alkyl transfer route is the most effective approach for 4, 6-DMDBT transformation, especially as the HYD pathway is hindered at high operating temperatures [14,15].

**Corresponding author:* Liu Li, *Dalian Research Institute of Petroleum and Petrochemicals, SINOPEC, Dalian, China*
E-mail addresses: liuli.fshy@sinopec.com
Received 2020-01-21, Received in revised form 2020-05-07, Accepted 2020-06-08, Available online 2020-08-31

In order to improve the HDS activity of the catalyst, the dynamics of the main steps in the HDS reaction should be studied. The computer modeling systems were developed to implement various mathematical models of HDS process [16,17]. The kineticss models based on model compounds were not applicable to the real feeds because of the complexity and mutual effects of the various components. For the industrial diesel feeds, a kineticss model including two regions of sulfur was developed by Guilian Wu. This model could describe the whole sulfur content range from 12,000 ppm to below 10 ppm; in addition, in the model, the mutual effects of sulfur compounds, nitrogen compounds, and aromatics were included [18].

For improving alkyl transfer reactivity, increasing the acid content of the catalyst is one of the effective methods, especially the Brönsted acid content [15,19]. ZSM-5 zeolites have high acid content, which is usually used in the hydrocracking catalysts [20]. In order to improve the alkyl transfer activity of the catalyst without reducing the yield of diesel oil, the catalyst should moderate acid content. In the paper, the catalytic performance and reaction kineticss of Mo-Co type catalysts supported on mesoporous ZSM-5 zeolite-alumina composites in the HDS of diesel feedstock are investigated.

Materials and Methods

Materials

Water glass solution (sodium silicate: $Na_2O{\cdot}4SiO_2$, SiO_2 24.6 wt.%, Na_2O 6.8 wt.%) was purchased from Zhejiang Tongxiang Water Glass Factory. Other chemicals of aluminum sulfate ($Al_2(SO_4)_3{\cdot}18H_2O$, 99%), nitric acid ($HNO_3$, 65%), tetrapropylammonium hydroxide (TPAOH, 25%), and cobalt nitrate ($Co(NO_3)_2{\cdot}6H_2O$, 99%) and ammonium heptamolybdate ($(NH_4)6Mo_7O_{24}{\cdot}4H_2O$, 99%) were purchased from Sinopharm Chemical Reagent Co., Ltd. The γ-Al_2O_3 powders and multi-hydroxyl compounds were purchased from the Fushun Catalysts Factory of SINOPEC. Aqueous solution (0.044 mol.L^{-1}) was slowly added. After further stirring for 2 h, the obtained aluminosilicate gel for dynamic crystallization at 180 °C for 36 h. After filtration and washing, the solid product was dried at 120 °C overnight, followed by calcination in air at 550 °C for 5 h. The γ-Al_2O_3 powders were provided by Fushun Catalysts Factory of SINOPEC. The mixture of Meso-ZSM-5, γ-Al_2O_3, nitric acid, and water was rolled, and then it was extruded into trefoil carrier precursors. The content of nitric acid and water in the mixture was 1.5 wt.% and 115%, respectively. The carrier precursor was dried at 110 °C for 3 h, and then it was calcinated 3h at 600 °C to produce supports. The carriers are referred to as DX-ZSM5 (X=12, 0) where X is the weight% of Meso-ZSM-5. The contrast support (D12-typical ZSM5) was prepared, and the typical ZSM-5 zeolite was synthesized according to the procedure reported in the literature [21].

The Co-Mo catalysts were prepared by impregnation with an aqueous solution of cobalt nitrate [$Co(NO_3)_2{\cdot}6H_2O$] and ammonium heptamolybdate [$(NH_4)6Mo_7O_{24}{\cdot}4H_2O$] with and without the addition of multi-hydroxyl compound. The loadings of Mo and Co oxides are 18 and 3 wt.%, respectively. The loading of the multi-hydroxyl compound is 5 wt.% in the catalysts. The resultant catalysts were then dried at 120 °C and calcined at 400 °C for 3 h. The catalysts are referred to as C12-ZSM5, C0-ZSM5, and C12-typical-ZSM5 catalysts.

Characterizations

The XRD patterns of the Meso-ZSM-5 and typical ZSM-5 zeolites were determined on a Rigaku Miniflex powder diffractometer with CuKα radiation (λ=0.154 nm).

N_2 physisorption was performed on a Micromeritics ASAP 2020 instrument at -196 °C. Each sample was heated to 300 °C under vacuum for 3 h before testing.

SEM measurements of the Meso-ZSM-5 and typical ZSM-5 zeolites were conducted on a JEM 7500F instrument operating at 0.1~30 kV.

NH_3-TPD was conducted as follows: the Meso-ZSM-5 and typical ZSM-5 zeolites after calcination were saturated with NH_3 for 30 min at 100 °C. Afterward, He was flushed to remove the physically adsorbed molecules. The TPD results were collected in He from 50 °C to 600 °C with a heating rate of 10 °C /min.

Py-adsorbed IR spectra were recorded on a PE FTIR Frontier instrument. The system was degassed at 500 °C for 5 h under vacuum, and then it was flushed by pure pyridine at room temperature for 20 min. The infrared (IR) spectra were then recorded.

The total sulfur of feedstock and products for measuring the total sulfur of feedstock and products by ANTEK 9000VLLS Sulfur Analyzer was calculated.

The catalytic performance (relative HDS activity) of the catalysts was obtained by the following formula:

Relative HDS activity (%) $=[1/Sp^{0.65}-1/Sf^{0.65}]\ /[1/Spr^{0.65}-1/Sf^{0.65}]\times100$,

where S_f, S_{pr}, and S_p represented the sulfur content of the feed, the sulfur content of products for reference catalyst, and the sulfur content of products for the experiment catalyst, respectively.

Catalyst Activity

The feedstock was a different diesel feedstock, and the properties are shown in Table 1. Studies were performed in a 200 ml fixed-bed reactor operating in batch mode. The flow diagram of the HDS reactor system is shown in Figure 1. The catalysts were subjected to sulfidation. Typically, the catalyst was placed in a reactor at 4 MPa of H_2 and heated to 110 °C. Subsidizing oil (96% kerosene and 4% CS_2) was then added into the reactor and maintained for 3 h. Afterwards, the reactor was heated to 320 °C for 8 h.

Reaction kineticss

The HDS reaction model is shown in Figure 2. S_1 was the easily removed sulfide, e.g., nonaromatic sulfur, thiophenes, and benzothiophene. S_1 was the sulfide having space steric and was removed hardly, e.g., alkyldibenzothiophenes (DBT), 4, 6-DMDBT. For S_1, compounds, the main reaction pathway was DDS by hydrogenolysis of the C-S bonds, where A corresponded to the compound after DDS reaction, k_2 represented the rate constant. For the S_{I1} compound, there were three reaction pathways: DDS, HYD, and alkyl transfer reaction, where B and C corresponded to the intermediate and the final compound of HYD reaction, k_2, and k_3 represented the rate constant of the forward and the reverse process.

Table 1 Properties of feedstock.

Analysis	Raw Oil for Model	Raw Oil for Experimental
D(20 °C)/g.cm^{-3}	0.853	0.852
Distillation Range/°C		
IBP/10%	217/277	220/279
30%/50%	296/309	295/310
70%/90%	327/356	328/359
95%/FBP	369/375	376/379
Sulfur Content/μg.g^{-1}	17750	18520
Nitrogen Content /μg.g^{-1}	138	529
Average Boiling Point T_V / °C	313.0	314.2
Mean Average Boiling Point T_M / °C	309.1	310.3
Molar Average Boiling Point Tr/ °C	305.8	295.9
Characteristic Factor K Value	11.85	11.87
API	33.61	33.80

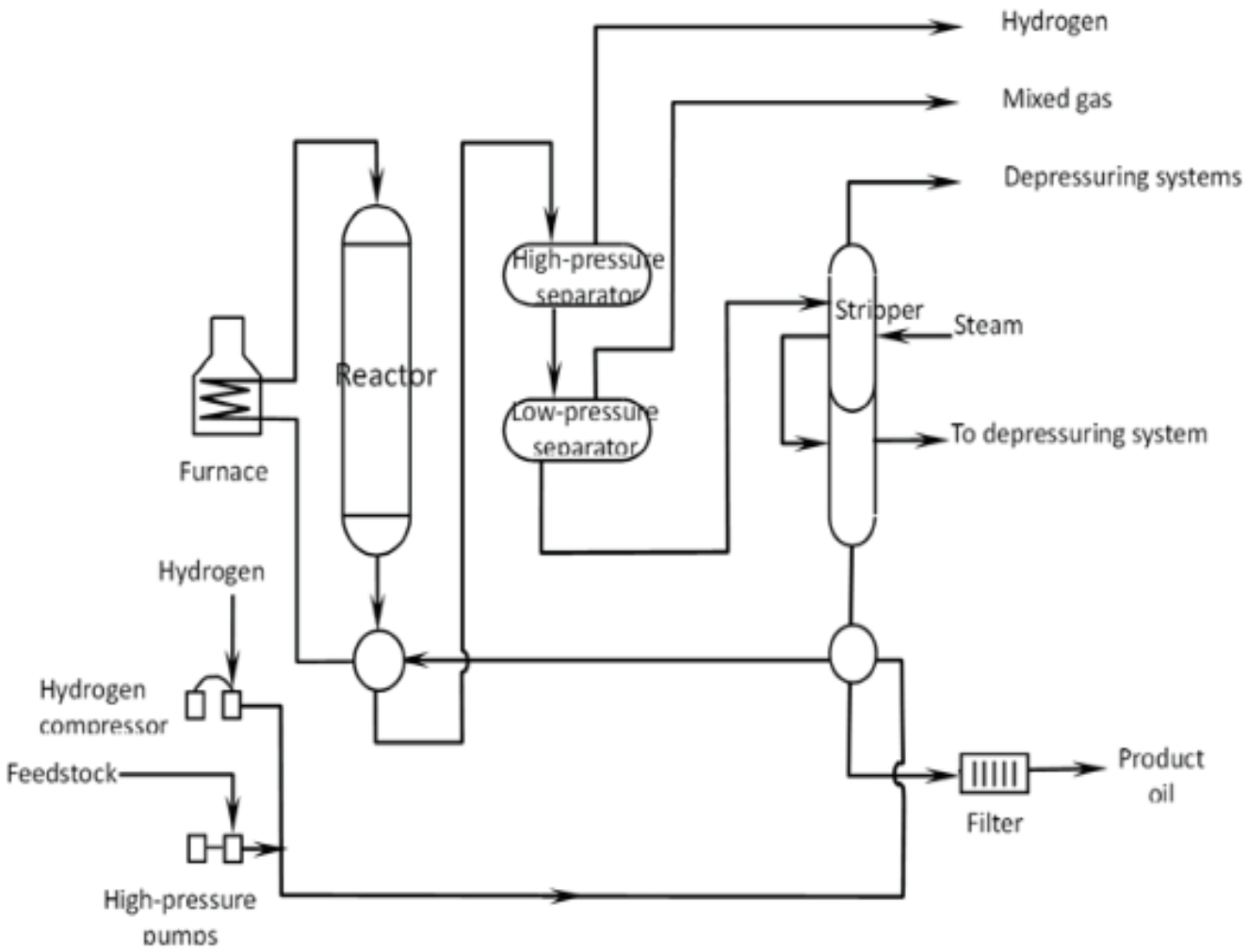

Fig. 1 Flow diagram of HDS reactor systems.

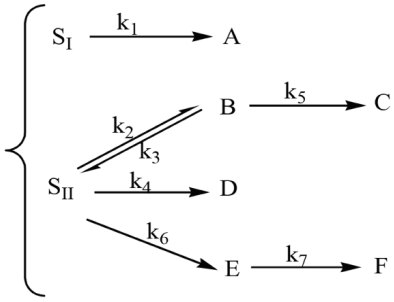

Fig 2 the HDS reaction model of different sulfide.

D corresponded to the compound after the DDS reaction, k_4 represented the rate constant. Also, E and F corresponded to the compound after alkyl transfer reaction and the final compounds, k_6 and k_7, represented the rate constant of alkyl transfer reaction and C–S bond scission reaction. The reaction order of each reaction pathway is assumed to be one order [17].

The differential equations of the HDS reaction are shown in Equation 1.

$$\begin{cases} -\dfrac{dC_{SI}}{dt} = k_1 C_{SI} \\ -\dfrac{dC_{SII}}{dt} = (k_2 + k_4 + k_6)C_{SII} - k_3 C_B \\ \dfrac{dC_B}{dt} = k_2 C_{SII} - (k_3 + k_5)C_B \\ \dfrac{dC_E}{dt} = k_6 C_{SII} - k_7 C_E \end{cases} \quad (1)$$

where C_i could be expressed by Equation 2:

$$\begin{cases} C_{SI} = C_{10}\exp(-k_1 t) \\ C_{SII} = \dfrac{1}{2\sqrt{R_2}}\left\{\left[C_{20}\left(\sqrt{R_2} - R_1\right) + 2k_3 C_{B0}\right]\exp\left(\dfrac{\sqrt{R_2} - R_3}{2LHSV}\right) + \left[C_{20}\left(R_1 + \sqrt{R_2}\right) - 2k_3 C_{B0}\right]\exp\left(\dfrac{-R_3 - \sqrt{R_2}}{2LHSV}\right)\right\} \\ C_B = \dfrac{1}{2\sqrt{R_2}}\left\{\left[C_{B0}\left(\sqrt{R_2} - R_4\right) + 2k_2 C_{20}\right]\exp\left(\dfrac{\sqrt{R_2} - R_3}{2LHSV}\right) + \left[C_{B0}\left(\sqrt{R_2} + R_4\right) - 2k_2 C_{20}\right]\exp\left(\dfrac{-R_3 - \sqrt{R_2}}{2LHSV}\right)\right\} \\ C_E = \dfrac{k_6 C_{SII}}{k_7 - k_6}[\exp(-k_6 t) - \exp(-k_7 t)] \\ C_S = C_{SI} + C_{SII} + C_B + C_E \end{cases} \quad (2)$$

where R_i could be expressed by Equation 3:

$$\begin{cases} R_1 = k_3 + k_5 - k_2 - k_4 - k_6 \\ R_2 = k_2^2 + k_3^2 + k_4^2 + k_5^2 + k_6^2 + 2(k_2k_3 + k_2k_4 + k_2k_6 + k_3k_5 + k_4k_6 - k_2k_5 - k_3k_4 - k_4k_5 - k_3k_6 - k_5k_6) \\ R_3 = k_2 + k_3 + k_4 + k_5 + k_6 \\ R_4 = k_2 + k_4 + k_6 - k_3 - k_5 \end{cases} \quad (3)$$

The rate constant could be expressed by Equation 4:

$$\begin{cases} k_1 = (mk_{10}(\dfrac{P}{6.0})^{\alpha} + n)\exp(-\dfrac{E_1}{RT}) \\ k_2 = (mk_{20}(\dfrac{P}{6.0})^{\beta} + n)\exp(-\dfrac{E_2}{RT}) \\ k_3 = (mk_{30}(\dfrac{P}{6.0})^{\chi} + n)\exp(-\dfrac{E_3}{RT}) \\ k_4 = (mk_{40}(\dfrac{P}{6.0})^{\delta} + n)\exp(-\dfrac{E_4}{RT}) \\ k_5 = (mk_{50}(\dfrac{P}{6.0})^{\varepsilon} + n)\exp(-\dfrac{E_5}{RT}) \\ k_6 = (mk_{60}(\dfrac{P}{6.0})^{\lambda} + n)\exp(-\dfrac{E_6}{RT}) \\ k_7 = (mk_{70}(\dfrac{P}{6.0})^{\theta} + n)\exp(-\dfrac{E_7}{RT}) \end{cases} \quad (4)$$

where m and n represent the corrected coefficient of the kinetics reaction model, P was operation hydrogen pressure, Ei represented the activation energy of different reactions, k_{10}~k_{70} represented the pre-exponential factors of the rate constant, and α, β, γ, δ, ε, λ, θ represented the index of hydrogen pressure. The Levenberg-Marquardt (LM) algorithm, also known as the damped least squares (DLS) method, was used to solve non-linear least squares problems in the paper.

Results and Discussion

Properties of Meso-ZSM-5 and Typical ZSM-5

The adsorption isotherms of meso-ZSM-5 and typical ZSM-5 in Figure 3 show that meso-ZSM-5 had obvious hysteresis loops, which indicated that the mesoporous structure was formed. In Figure 4, the pore distribution of the meso-ZSM-5 and typical ZSM-5 is shown. The most probable apertures of meso-ZSM-5 was 2 nm and 20 nm. In addition, the mesoporous structure of meso-ZSM-5 in comparison with typical ZSM-5 was obvious, and external specific surface area and pore volume of meso-ZSM-5 were higher, as shown in Table 2. The specific surface area and pore volume of meso-ZSM-5 and typical ZSM-5 were lower than that of γ-Al_2O_3.

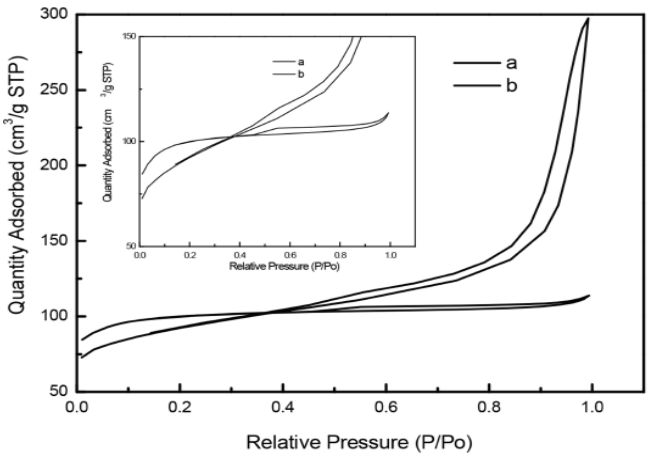

Fig 3 The adsorption isotherms of (a) Meso-ZSM-5 and (b) typical ZSM-5 (b).

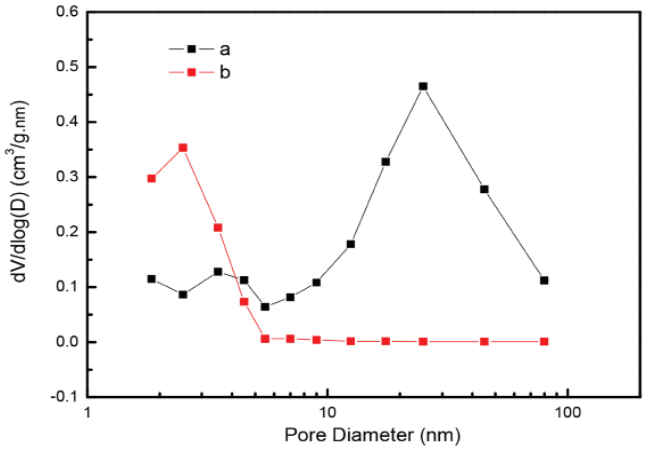

Fig. 4 The pore distribution of (a) Meso-ZSM-5 and (b) typical ZSM-5.

Table 2 The porous properties of meso-ZSM-5 and typical ZSM-5.

sample	S_{BET}/($m^2.g^{-1}$)	microporous S_{BET}/ ($m^2.g^{-1}$)	external S_{BET}/ ($m^2.g^{-1}$)	V_p/ ($cm^3.g^{-1}$)	microporous V_p/ ($cm^3.g^{-1}$)
typical ZSM-5	379	288	92	0.17	0.11
meso-ZSM-5	336	180	156	0.40	0.07
γ-Al_2O_3	400	_	_	0.91	_

In Figure 5, the SEM images of the meso-ZSM-5 and typical ZSM-5 are shown. The 100 nm small particles accumulated to form 5000 nm large particles in the meso-ZSM-5, and there were many pores between the small particles, which provided more space and active sites for the reaction compared with typical ZSM-5 having regular cuboid structure over 500 nm.

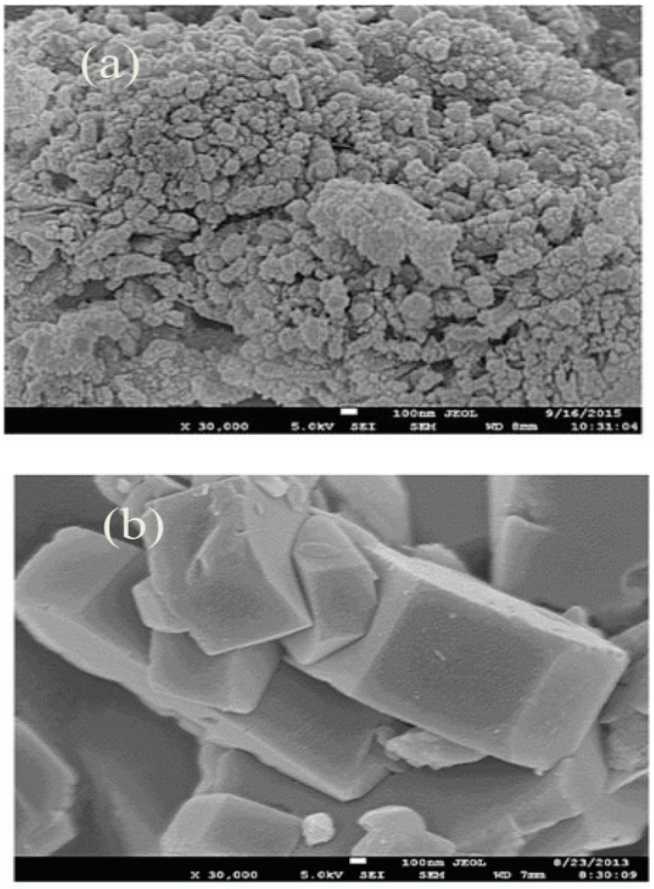

Fig. 5 The SEM image of (a) Meso-ZSM-5 and (b) typical ZSM-5.

The crystallinity of zeolite can significantly influence the porosity and acid properties of corresponding catalysts. In Figure 6, the XRD patterns of the meso-ZSM-5 and typical ZSM-5 are shown. The crystallinity of meso-ZSM-5 was lower than that of typical ZSM-5. According to the results of XRD, BET, and SEM, the porosity of meso-ZSM-5 is closely related to its incomplete crystallization.

The Lewis and Brönsted sites of the two catalysts are determined by Py-IR. The bands at 1445 and 1556 cm^{-1} are attributed to the pyridine chemisorbed on Lewis sites and the vibration mode of pyridinium ions adsorbed on Brönsted sites, respectively [22]. In addition, the pyridine adsorbed on both Lewis and Brönsted sites shows up at 1486 cm^{-1}. The acidic amount of zeolites are listed in Table 3. The total and Brönsted acid amount of meso-ZSM-5 was lower than that of typical ZSM-5. However, the Lewis acid amount of meso-ZSM-5 was higher compared to typical ZSM-5 due to incomplete crystallization of meso-ZSM-5. Furthermore, the total acid amount of typical-ZSM-5 was high, which it would cause a cracking reaction and decrease the diesel product yield [20].

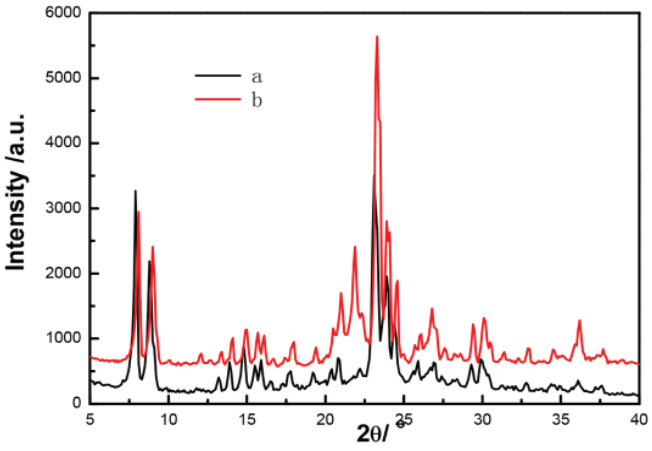

Fig. 6 The XRD patterns of (a) meso-ZSM-5 (b) and typical ZSM-5.

Table 3 The Py-IR acid properties of meso-ZSM-5 and typical ZSM-5.

Samples	Total acidic amount/ (mmol. g^{-1})	Acidic amount/(mmol. g^{-1})		$n(SiO_2)/n(Al_2O_3)$
		B	L	
meso-ZSM-5	0.319	0.120	0.199	49.0
Typical ZSM-5	0.632	0.499	0.133	49.0

The porosity and Acid Properties of Supports

The porosity and acid properties of supports depend on that of catalysts. In Table 4, the porosity and acid properties of carriers are shown. Compared with D0-ZSM5 carriers, the V_P and D_P of D12-ZSM5 and D12-typical-ZSM5 carriers were lower, because those of meso-ZSM-5 and typical ZSM-5 were lower than that of γ-Al_2O_3 (The specific surface area, pore-volume, and diameter of γ-Al_2O_3 powder are 400 $m^2.g^{-1}$, 0.91 $cm^3.g^{-1}$, and 9.1 nm.). The V_P and D_P of D12-ZSM5 were higher than that of D12-typical-ZSM5 because meso-ZSM-5 had a large amount of mesoporous. The DP of D12-typical-ZSM5 of 5.6 nm was small, which may hinder the diffusion of macromolecular sulfides.

Compared with D0-ZSM5 carriers, the Brönsted and Lewis acidic amount were all a little higher. Properly, increasing the acid content of the support, especially the Brönsted acidic amount, can improve the alkyl transfer activity and the HDS activity of the catalyst, without reducing the yield of diesel oil.

Table 4 The porous and Py-IR acid properties of carriers.

Carriers	V_P/ ($cm^3.g^{-1}$)	S_{BET}/($m^2.g^{-1}$)	D_P / nm	Total acidic amount/($mmol.g^{-1}$)	Acidic amount/($mmol.g^{-1}$)	
					B	L
D12-ZSM5	0.59	327	7.2	0.512	0.073	0.439
D0-ZSM5	0.61	334	7.4	0.415	0.037	0.378
D12-typical ZSM5	0.52	353	5.9	0.735	0.223	0.512

The Performance of the Catalysts

Compared with the C0-ZSM5 catalyst, the V_P and D_P of C12-ZSM5 and C12-typical-ZSM5 catalysts (shown in Table 5) were lower because those of meso-ZSM-5 and typical ZSM-5 were lower than that of γ-Al_2O_3. The V_P and D_P of C12-ZSM5 were higher than that of C12-typical-ZSM5 because meso-ZSM-5 had a large amount of mesoporous. The DP of C12-typical-ZSM5 of 4.7 nm was small, which may hinder the diffusion of macromolecular sulfides.

The operation condition was 370 °C, a hydrogen pressure of 6.4 MPa, 1.5 h^{-1} space velocities, and a volume ratio of hydrogen to the oil of 500. The crude oil was an experimental diesel feedstock. The HDS activity of the catalysts is shown in Table 5. Compared with C0-ZSM5 catalysts, the relative HDS activity of C12-ZSM5 was higher. The acid content of the support of the C12-ZSM5 catalyst was higher than that of support of C0-ZSM5, especially the Brönsted acidic amount, which may improve the alkyl transfer activity. Although the acid content of support of the C12-typical ZSM5 was highest, the VP and DP of support of the C12-typical ZSM5 were smallest compared with that of C0-ZSM5 and C12-ZSM5 catalysts. The smaller VP and DP may block macromolecular sulfide diffusion, which could lead to low HDS activity.

DDS and HYD Reaction Routes on C12-ZSM5 Catalyst

At low operating temperatures, the dominated pathways of S_I and S_{II} compound removal were DDS, HYD, and DDS routes over the catalyst, respectively. The operation condition was 340 °C, a hydrogen pressure of 4.0 MPa, and different space velocities. The experimental and simulated sulfur content is shown in Figure 7, and the residual sum of squares was equal to 0.073. In Figure 7, the sulfur content increased with an increase in space velocities is shown.

The rate constant under 340 °C was simulated and k_i (i=1, 2, 3, 4, 5) was 33.4×10^{-3}, 2.7×10^{-3}, 1.5×10^{-3}, 0.2×10^{-3} and 12.7×10-3 $mol.g^{-1}.s^{-1}$ respectively. The sulfur content decreased with an increase in the operating temperatures, as seen in Figure 8. The simulated sulfur content at a hydrogen pressure of 4.0 MPa, a space velocity of 1.5 h^{-1}, and different operating temperatures was consistent with experimental results, and the residual sum of squares was 0.02. The activation energy of DDS and HYD reactions was simulated, and Ei (i=1, 2, 3, 4, 5) were 71.29, 57.06, 77.88, 156.29, and 84.90 $kJ.mol^{-1}$, respectively. The pre-exponential factors of rate constant ki0 (i=1, 2, 3, 4, 5) were 3.98×10^7, 1.99×10^5, 6.58×10^6, 3.56×10^{12}, and 2.18×108, respectively. The index of hydrogen pressure α, β, γ, δ, and ε was 0.01, 5.9, -0.9, 0.2 and 0.7 respectively.

The activation energy of DDS reaction E4 (156.29 $kJ.mol^{-1}$) was greatly higher than that of HYD reaction E2 (57.06 $kJ.mol^{-1}$), which it indicated that the HYD reaction route appeared to be of great importance for the removal of alkyldibenzothiophenes, and it was the main route at low operating temperatures. However, the HYD reaction was an exothermic reaction, which would be limited at high operating temperatures because of thermodynamic equilibrium limitations [8,9].

Table 5 The porous properties and relative HDS activity of the catalysts

Catalyst	V_P/ ($cm^3.g^{-1}$)	S_{BET}/($m^2.g^{-1}$)	D_P/nm	w(S)/ ppm	Relative HDS activity，%
C12-ZSM5	0.36	263	5.5	6.9	147
C0-ZSM5	0.41	285	5.8	12.5	100
C12-typical ZSM5	0.34	292	4.7	18.5	77

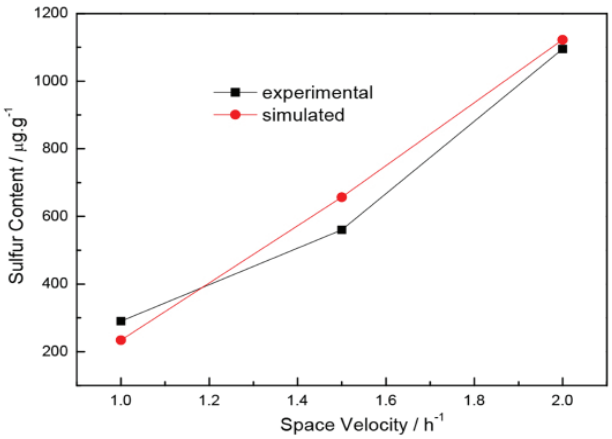

Fig 7 The experimental and simulated sulfur content at different space velocities 340 °C and 4.0 MPa.

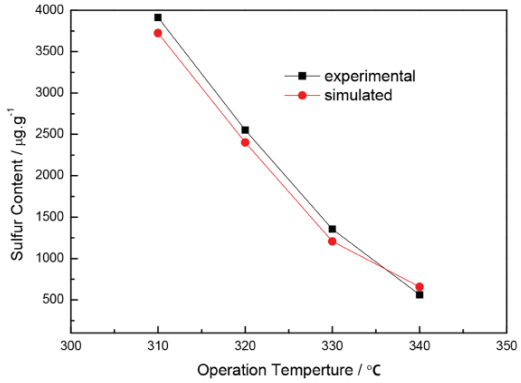

Fig. 8 The experimental and simulated sulfur content at low operating temperatures, 4.0 MPa, and 1.5 h^{-1}.

Alkyl Transfer Reaction Route on C12-ZSM5 Catalyst

At low operating temperatures, the alkyl transfer route for ultra-deep diesel HDS reaction on the Mo-Co type catalyst could be ignored, and the dominated routes of S_{II} compounds removal were HYD and DDS according to our previous researches [14,15]. Moreover, it is found out that HYD, DDS, and alkyl transfer pathways were the main routes at high operating temperatures. By following this conclusion, the hypothesis, i.e. the kinetics parameters of DDS and HYD routes, were the same at the different operating temperatures is proposed. At high operating temperatures, the content of sulfur removal through HYD and DDS routes was calculated by the above models, and the content of sulfur removal through the alkyl transfer HDS route could be calculated by subtracting the experimental result from the simulated result. Afterwards, the model parameters of the alkyl transfer desulfurization reaction route were simulated. The content of sulfur removal through the alkyl transfer HDS route under a hydrogen pressure of 4.0 MPa, a volume ratio of hydrogen to the oil of 500, 390 °C, and different space velocities is shown in Figure 9.

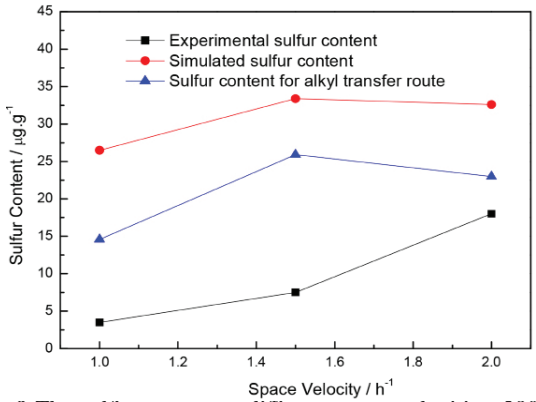

Fig. 9 The sulfur content at different space velocities, 390 °C and 4.0 MPa according to HYD, DDS and alkyl transfer routes.

The results showed that the content of sulfur removal through the alkyl transfer route greatly increased with an increase in space velocities, whereas it decreased when the space velocity was over 1.5 h^{-1}. The content of sulfur removal through the alkyl transfer HDS route under a hydrogen pressure of 4.0 MPa or 6.4 MPa, a volume ratio of hydrogen to the oil of 500, a space velocity of 1.5 h^{-1} and high temperatures is shown in Figures 10 and 11.

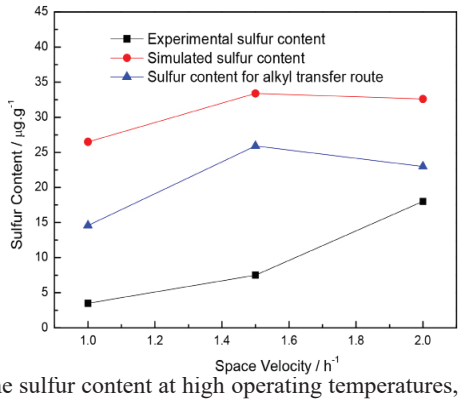

Fig. 10 The sulfur content at high operating temperatures, 4.0 MPa and 1.5 h^{-1} according to HYD, DDS and alkyl transfer routes.

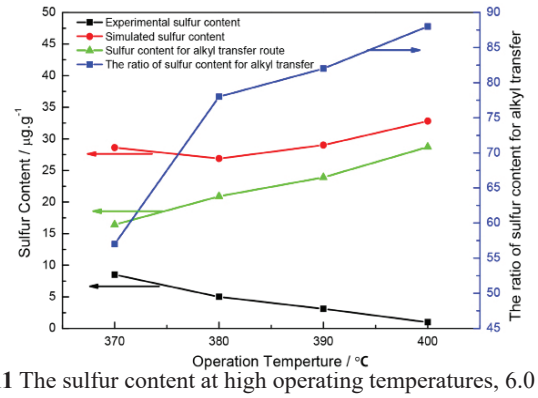

Fig. 11 The sulfur content at high operating temperatures, 6.0 MPa, and 1.5 h^{-1} according to HYD, DDS and alkyl transfer routes.

The results showed that the content of sulfur removal through alkyl transfer route greatly increased with an increase in the operating temperatures, and the ratio of the content of sulfur removal through alkyl transfer route at 4.0 MPa and at 370 °C, 380 °C, 390 °C and 400 °C was 50%, 67%, 78%, and 86% respectively. Moreover, the ratio of the content of sulfur removal through alkyl transfer route at 6.4 MPa and at 370 °C, 380 °C, 390 °C and 400 °C was 57%, 78%, 82%, and 88% respectively. The results implied that the alkyl transfer route was significant at high operating temperature, and its pathway was dominated as the sulfur content of feedstock was less than 50 ppm.

The kinetics parameters of the alkyl transfer desulfurization reaction route were simulated, and the obtained results are shown in Table 6. The results showed that the activation energy of alkyl transfer reaction E6 (114.39 kJ·mol^{-1}) was lower than that of DDS reaction (156.29 kJ·mol^{-1}), and it was higher than that of HYD reaction (57.06 kJ·mol^{-1}), whereas the E7 of alkyl transfer route (80.29 kJ·mol^{-1}) was lower than E5 of HYD route (84.90 kJ·mol^{-1}). The results indicated that the S_{II} compounds were transformed easier according to the alkyl transfer pathway than the DDS route.

Table 6 Model parameters of the alkyl transfer desulfurization reaction route.

Parameter	Value
k_{60}	3.18×10^{9}
k_{70}	5.94×10^{7}
E_{6}/ kJ·mol^{-1}	114.39
E_{7} /kJ·mol^{-1}	80.29
λ	0.1
θ	0.8

According to the above simulating, the model of HDS reaction on the C12-ZSM5 catalyst was established in the HDS of diesel feedstock and expressed by Equation 5.

$$\begin{cases} k_1 = (m \times 3.98 \times 10^6 \times \left(\frac{p}{6.0}\right)^{0.01} + n)\exp(-\frac{71292}{RT}) \\ k_2 = (m \times 1.99 \times 10^5 \times \left(\frac{p}{6.0}\right)^{5.91} + n)\exp(-\frac{57059}{RT}) \\ k_3 = (m \times 6.58 \times 10^6 \times \left(\frac{p}{6.0}\right)^{-0.9} + n)\exp(-\frac{77876}{RT}) \\ k_4 = (m \times 3.56 \times 10^{12} \times \left(\frac{p}{6.0}\right)^{0.16} + n)\exp(-\frac{156287}{RT}) \\ k_5 = (m \times 2.18 \times 10^8 \times \left(\frac{p}{6.0}\right)^{0.7} + n)\exp(-\frac{84902}{RT}) \\ k_6 = (m \times 3.18 \times 10^9 \times \left(\frac{P}{6.0}\right)^{0.1} + \mathrm{n})\exp(-\frac{114392}{RT}) \\ k_7 = (m \times 5.94 \times 10^7 \times \left(\frac{P}{6.0}\right)^{0.8} + n)\exp(-\frac{80288}{RT}) \end{cases} \quad (5)$$

The corrected coefficient of the kinetics model m and n was in connection with densities and average boiling points of feedstock and expressed by Equation 6.

$$\begin{cases} m = (\dfrac{\text{average boiling point of model}}{\text{average boiling point of experiment}})^4 \\ n = 0.118 \times (API_{\text{experimental oil}} - API_{\text{model oil}}) \end{cases} \quad (6)$$

In order to validate the model, the HDS reaction of the different diesel feedstock on the C12-ZSM5 catalyst was simulated. According to Equation 6, the value of m and n was 0.98 and 0.022 for the experimental diesel feedstock, respectively.

The experimental and simulated sulfur content of the product at different operation conditions are shown in Figures 12 and 13. The results showed that the calculated results were in good agreement with the experimental results, and the residual sum of squares was 0.56, which indicated that the kinetics model was reasonable and accurate. In Figure 12, the experimental and simulated sulfur content at different temperatures, 6.4 MPa, a space velocity of 1.5 h^{-1}, and a volume ratio of hydrogen to the oil of 500 is shown. The sulfur content of the product decreased with an increase in the operating temperature, and it was 11.5 ppm at 360 °C. The experimental and simulated sulfur content of the product diesel at different hydrogen pressures, 360 °C, a volume ratio of hydrogen to the oil of 500, and a space velocity of 1.5 h^{-1} is shown in Figure 13. The results showed that the calculated results were in good agreement with the experimental results, and the sulfur content of the product increased with an increase in the hydrogen pressure that was 11.5 and 60 ppm at 6.4 and 4.0 MPa, respectively. It indicated that increasing the hydrogen pressure would significantly improve the transformation ratio of sulfides.

The sulfur content of product diesel after ultra-deep HDS was 11.5 ppm at operation condition: 360 °C, 6.4 MPa, 1.5 h^{-1} and a volume ratio of hydrogen to the oil of 500, which did not meet requirements of the China National V and Euro V standards (< 10 ppm sulfur). In order to meet requirements, the appropriate operating conditions should be simulated using the kinetics models to reduce the sulfur content of product diesel. The simulated result showed that sulfur content was 7.6 ppm at 370 °C, 6.4 MPa, 1.5 h^{-1}, and a volume ratio of hydrogen to the oil of 500, which was in good agreement with the experimental result. The developed catalyst with the proposed kinetics models on sulfur removal from diesel would contribute to the application of the diesel hydrotreating process, and provide guidance on commercial applications.

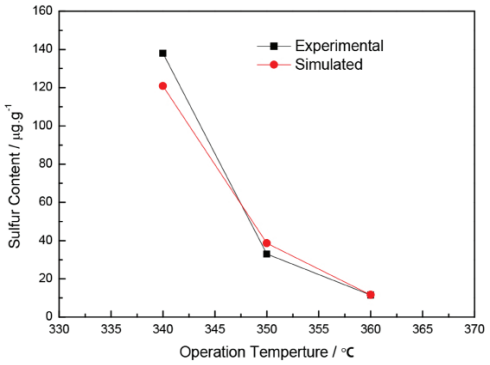

Fig. 12 The experimental and simulated sulfur content of the product diesel at different temperatures, 6.4 MPa and a space velocity of 1.5 h^{-1}.

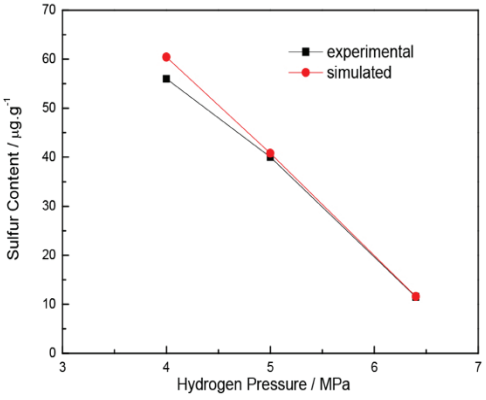

Fig. 13 The experimental and simulated sulfur content of the product diesel at different hydrogen pressures, 360 °C and a space velocity of 1.5 h^{-1}.

Conclusions

The external specific surface area and pore volume of meso-ZSM-5 were higher, compared with typical ZSM-5, and the 100 nm small particles accumulated to form 5000 nm large particles in the meso-ZSM-5. There were also many pores between the small particles, which provided more space and active sites for the reaction compared with typical ZSM-5 having a regular cuboid structure over 500 nm.

The VP and DP of D12-ZSM5 carriers were higher than that of D12-typical-ZSM5 carriers because meso-ZSM-5 had a large amount of mesoporous. The relative HDS activity of C12-ZSM5 catalyst was highest because it had large V_p and D_p, and moderate acid content, which could improve the alkyl transfer activity and the macromolecular sulfide diffusion.

The seven lumped kinetics equations containing HYD, DDS, and alkyl transfer reaction mechanisms were established to further research the dynamics of diesel ultra-deep HDS reactions on the C12-ZSM5 catalyst. The calculated sulfur contents were in good agreement with the experimental results, and the residual sum of squares was 0.56, indicating the kinetics model was reasonable and accurate. The results showed that the HYD reaction route was limited at

high operating temperatures because of thermodynamic equilibrium limitations. The activation energy of alkyl transfer reaction E6 (114.39 kJ·mol^{-1}) was lower than that of DDS reaction (156.29 kJ·mol^{-1}), and it was higher than that of HYD reaction (57.06 kJ·mol^{-1}), whereas the E7 of alkyl transfer route (80.29 kJ·mol^{-1}) was lower than E5 of HYD route (84.90 kJ·mol^{-1}).

The results indicated alkyldibenzothiophenes transformation was easier according to the alkyl transfer pathway than the DDS route because of steric hindrance. By increasing the operating temperatures, the content of sulfur removal through the alkyl transfer route greatly increased. In addition, the ratios of the content of sulfur removal through alkyl transfer at 400 °C and 4.0 MPa or 6.0 MPa were 86% or 88%, respectively. It indicated that the alkyl transfer route was significant at high operating temperature, and its pathway dominated when the sulfur content of feedstock was less than 50 ppm. Ultimately, the developed catalyst with the proposed kinetics models on sulfur removal from diesel would contribute to the application of the diesel hydrotreating process, and guide commercial applications.

Acknowledgments

This study was financially supported by the Ministry of Science and Technology of China (No.YS2017YFGX010180) and Scientific Research Fund of SINOPEC (No. 118008).

Nomenclatures

HDS: Hydrodesulfurization
DDS: Direct desulfurization
DLS: Damped least squares
LM: Levenberg-Marquardt algorithm

References

1. Kagami N, Vogelaar B M, Langeveld A D (2005) Reaction pathways on NiMo/Al_2O_3 catalysts for hydrodesulfurization of diesel fuel, Applied Catalysis A, 93:11-23.
2. Bouwens A M, Vanzon F B M, Vandijk M P (1994) On the structural differences between alumina-supported comos type I and alumina-, silica-, and carbon-supported comos type II phases studied by XAFS, MES, and XPS, Journal of Catalysis, 146: 375-393.
3. Hensen E J M, Kooyman P J, Meer Y (2001) The relation between morphology and hydrotreating activity for supported MoS_2 particles original research article, Journal of Catalysis,199:224-235.
4. Narinobu K, Bas M V, Langeveld A D (2005) Reaction pathways on NiMo/Al_2O_3 catalysts for hydrodesulfurization of diesel fuel, Applied Catalysis A, 293:11-23.
5. Laurtsen J V, Besenbacher F (2015) Atom-resolved scanning tunneling microscopy investigations of molecular adsorption on MoS_2 and CoMoS hydrodesulfurization Catalysts, J. Catal., 328:49-58.
6. Zepeda T A (2008) Comparison and performance of different sulphided Ti-loaded mesostructured silica-supported CoMo catalysts in deep HDS, Applied Catalysis A, 347:148-161.
7. Pawelec B, Fierro J L G, Montesinos A (2008) Influence of the acidity of nanostructured CoMo/P/Ti-HMS catalysts on the HDS of 4,6-DMDBT reaction pathways, Journal of Applied Catalysis B: Environmental, 80(1-2):1-14.
8. Walton A S, Lauritsen J V, Topsoe H (2013) MoS_2 nanoparticle morphologies in hydrodesulfurization catalysis studied by scanning tunneling microscopy, Journal of Catalysis, 308:306-318.
9. Macaud M, Milenkovic A, Schulz E, et al. (2000) Hydrodesulfurization of Alkyldibenzothiophenes: Evidence of Highly Unreactive Aromatic Sulfur Compounds, Journal of Catalysis, 193: 255–263.
10. Meille V, Schulz E, Lemaire M, et al. (1997) Hydrodesulfurization of Alkyldibenzothiophenes over a NiMo/Al_2O_3 Catalyst: Kinetics and Mechanism, Journal of Catalysis, 170: 29–36.
11. Houalla M, Broderick D, Sapre A V, et al. (1994) "Hydrodesulfurization of methyl-substituted dibenzothiophenes catalyzed by sulfided Co-Mo\γ-Al_2O_3, Journal of Catalysis, 61(2): 523-527.
12. Meille V, Schulz E, Lemaire M, et al. (1997) Hydrodesulfurization of Alkyldibenzothiophenes over a NiMo/Al_2O_3 Catalyst: Kinetics and Mechanism," Journal of Catalysis, 170, 29-36.
13. Ramirez J, Fuentes S, Díaz G, et al. (1989) Hydrodesulphurization activity and characterization of sulphided molybdenum and cobalt-molybdenum catalysts: Comparison of Alumina-, Silica-Alumina- and Titania-Supported Catalysts, Applied Catalysis, 52: 221-224.
14. Fang X C, Guo R, Yang C M (2013) The development and application of catalysts for ultra-deep hydrodesulfurization of diesel, Chinese Journal of Catalysis, 34: 130-139.
15. Peng C, Guo R, Feng X (2019) Tailoring the structure of Co-Mo/mesoporous γ-Al_2O_3 catalysts by adding multihydroxyl compound: A 3000 kt/a industrial-scale diesel ultra-deep hydrodesulfurization study," Chemical Engineering Journal, 377: 119706-119733.
16. Krivtcova N I, Tataurshikov A A, Ivanchina E D, Krivtsov E B (2015) Mathematical Modelling of Diesel Fuel Hydrodesulfurization Kinetics, Procedia Chem., 15: 180–186.
17. Ganguly S K (2013) Kinetics of Hydrodesulfurization of Diesel: Internal Mass Transfer Aspects, Journal of Petroleum Science and Technology, 31: 672–679.
18. Wu G, Yin Y, Chen W, et al. (2020) Catalytic kinetics for ultra-deep hydrodesulfurization of diesel, Journal of Chemical Engineering Science, 214, 115446.
19. Ding L H, Zheng Y, Zhang Z H, Lu Y, Qin K, Zhang L, Song Y and Li M (2006) Hydrotreating of light cycled oil using WNi/Al_2O_3 catalysts containingzeolite beta and/or chemically treated zeolite Y," Journal of Catalysis, 241:435–445.
20. Jiang J, Yang C, Lu Z, Ding J, Li T, Lu Y, Cao F, (2015) Characterization and application of a Pt/ZSM-5/SSMF catalyst for hydrocracking of paraffin wax, Catalysis Communications, 60: 1-4.
21. Yu Q Y, Zhang L, Guo R (2017) Catalytic performance of CoMo catalysts supported on mesoporous ZSM-5 zeolite-alumina composites in the hydrodesulfurization

of 4, 6-dimethyldibenzothiophene, Journal of Fuel Processing Technology, 159: 76-87.
22. Kwak C, Lee J J, Bae J S, Moon S H (2001) Poisoning effect of nitrogen compounds on the performance of $CoMoS/Al_2O_3$ catalyst in the hydrodesulfurization of dibenzothiophene, 4-methyldibenzothiophene, and 4, 6-dimethyldibenzothiophene," Journal of Applied Catalysis B: Environmental, 35: 59-68.